

ATLAS lifts the Cup: discovery of a new Milky Way satellite in Crater^{★†}

V. Belokurov,^{1,‡} M. J. Irwin,¹ S. E. Koposov,^{1,2} N. W. Evans,¹ E. Gonzalez-Solares,¹
N. Metcalfe³ and T. Shanks³

¹*Institute of Astronomy, Madingley Rd, Cambridge CB3 0HA, UK*

²*Sternberg Astronomical Institute, Moscow State University, Universitetskii pr. 13, Moscow 119991, Russia*

³*Department of Physics, Durham University, South Road, Durham DH1 3LE, UK*

Accepted 2014 March 27. Received 2014 March 25; in original form 2014 March 13

ABSTRACT

We announce the discovery of a new Galactic companion found in data from the ESO VST ATLAS survey, and followed up with deep imaging on the 4-m William Herschel Telescope. The satellite is located in the constellation of Crater (the Cup) at a distance of ~ 170 kpc. Its half-light radius is $r_h = 30$ pc and its luminosity is $M_V = -5.5$. The bulk of its stellar population is old and metal poor. We would probably have classified the newly discovered satellite as an extended globular cluster were it not for the presence of a handful of blue loop stars and a sparsely populated red clump. The existence of the core helium burning population implies that star formation occurred in Crater perhaps as recently as 400 Myr ago. No globular cluster has ever accomplished the feat of prolonging its star formation by several Gyr. Therefore, if our hypothesis that the blue bright stars in Crater are blue loop giants is correct, the new satellite should be classified as a dwarf galaxy with unusual properties. Note that only 10° to the north of Crater, two ultrafaint galaxies Leo IV and Leo V orbit the Galaxy at approximately the same distance. This hints that all three satellites may once have been closely associated before falling together into the Milky Way halo.

Key words: Stars: Hertzsprung–Russell and colour–magnitude diagrams – Galaxy: fundamental parameters – Galaxy: globular clusters: general – Galaxy: halo – Galaxies: dwarf.

1 INTRODUCTION

By revealing 20 new satellites in the halo of the Milky Way (Willman et al. 2005a,b; Belokurov et al. 2006, 2007, 2008, 2009, 2010; Zucker et al. 2006a,b; Irwin et al. 2007; Koposov et al. 2007; Walsh, Jerjen & Willman 2007; Grillmair 2009; Balbinot et al. 2013), the Sloan Digital Sky Survey (SDSS) has managed to blur the boundary between what only recently seemed two entirely distinct types of objects: dwarf galaxies and star clusters. As a result, we now appear to have ‘galaxies’ with a total luminosity smaller than that of a single bright giant star (e.g. Segue 1, Ursa Major II). The SDSS observations also wrought havoc on intraclass nomenclature, giving us dwarf spheroidals with properties of dwarf irregulars, i.e. plenty of gas and recent star formation (e.g. Leo T) as well as distant halo globulars so insignificant that if they lay 10 times closer they would surely be called open clusters (e.g. Koposov 1 and 2).

The art of satellite classification, while it may seem like idle pettifoggery, is nonetheless of importance to our models of structure formation. By classifying the satellite, on the basis of all available observational evidence, as a dwarf galaxy, we momentarily gloss over the details of its individual formation and evolution, and instead move on to modelling the population as a whole. We believe there are more than 20 dwarf galaxies in the Milky Way environs and predict that there are tens more dwarf galaxies waiting to be discovered in the near future (see e.g. Koposov et al. 2008; Tollerud et al. 2008). It is worth pointing out that the cold dark matter (CDM) paradigm remains the only theory that can easily produce large numbers of dwarf satellites around spirals like the Milky Way or the M31. So far the crude assumption of all dwarf galaxies being simple clones of each other living in similar dark matter subhaloes has paid off and the Λ CDM paradigm appears to have been largely vindicated (e.g. Koposov et al. 2009). However, as the sample size grows, new details emerge and may force us to reconsider this picture.

The distribution of known satellites around the Milky Way is anisotropic, though this is partly a consequence of selection effects. It has been claimed that the Galactic satellites form a vast disc-like structure about 40 kpc thick and 400 kpc in diameter, and that this is inconsistent with Λ CDM (e.g. Kroupa, Pawlowski & Milgrom 2012). In fact, as the recent discoveries have been made using the SDSS, a congregation of satellites in the vicinity of

[★]Based on data products from observations made with ESO Telescopes at the La Silla Paranal Observatory under public survey programme ID programme 177.A-3011(A,B,C).

[†]Based in part on service observations made with the WHT operated on the island of La Palma by the Isaac Newton Group in the Spanish Observatorio del Roque de los Muchachos of the Instituto de Astrofísica de Canarias.

[‡]E-mail: vasily@ast.cam.ac.uk

the north Galactic cap is only to be expected (Belokurov 2013). Even then, anisotropic distributions of satellite galaxies do occur naturally within the Λ CDM framework. For example, using high-resolution hydrodynamical simulations, Deason et al. (2011) found that roughly 20 per cent of satellite systems exhibit a polar alignment, reminiscent of the known satellites of the Milky Way galaxy. In 10 per cent of these systems there was evidence of satellites lying in rotationally supported discs, whose origin can be traced back to group infall. Significant fractions of satellites may be accreted from a similar direction in groups or in loosely bound associations and this can lead to preferred planes in the satellite distributions (e.g. D’Onghia & Lake 2008; Li & Helmi 2008). There is ample evidence of such associations in the satellites around the Milky Way – such as Leo IV and Leo V (de Jong et al. 2010) – and M31 – such as NGC 147 and NGC 185 and possibly Cass II (Fattahi et al. 2013; Watkins, Evans & van de Ven 2013).

Understanding how dwarf galaxies and clusters evolve in relation to their environment remains a challenge. These objects can occupy both low- and high-density environments and are subject to both internal processes (mass segregation, evaporation and ejection of stars, bursts of star formation) and external effects [disruption by Galactic tides, disc and bulge shocking, ram pressure stripping of gas by the interstellar medium (ISM)]. There is also growing evidence for interactions and encounters of satellites with each other, for example, in the tidal stream within And II (Amorisco, Evans & van der Ven 2014) and the apparent shells around Fornax (Coleman et al. 2004; Amorisco & Evans 2012). The variety of initial conditions near the time of formation, together with the diversity of subsequent evolutionary effects in a range of different environments, is capable of generating a medley of objects with luminosities and sizes of the present day cluster and dwarf galaxies populations. It is therefore unsurprising that as the Milky Way halo is mapped out we are finding an increasing number of ambiguous objects that does not fit tidily into the once clear-cut categories of clusters and dwarf galaxies.

In this paper, we describe how applying the overdensity search algorithms perfected on the SDSS data sets to the catalogues supplied by the VST ATLAS survey has uncovered a new satellite in the constellation of Crater. Although Crater has a size close to that of globular clusters (GCs), we believe that the satellite has had an extended star formation history and therefore should be classified as a galaxy (see e.g. Willman & Strader 2012). Therefore,

following convention, it is named after the constellation in which it resides. Section 2 gives the particulars of the ATLAS data and of the follow-up imaging we have acquired with the 4-m William Herschel Telescope (WHT). Section 3 describes how the basic properties of Crater were estimated. Section 4 provides our discussion and conclusions.

2 DATA, DISCOVERY AND FOLLOW-UP

2.1 VST ATLAS

ATLAS is one of the three ESO public surveys currently being carried out at Paranal in Chile with the 2.6-m VLT Survey Telescope (VST). ATLAS aims to cover a wide area of several thousand square degrees in the southern celestial hemisphere in five photometric bands, *ugriz*, to depths comparable to those reached by the SDSS in the north. Compared to the SDSS, ATLAS images have finer pixel sampling and somewhat longer exposures, while the median seeing at Paranal is slightly better than that at Apache Point. We note that the resulting default catalogued photometry produced by the Cambridge Astronomical Survey Unit (CASU) is in the Vega photometric system rather than AB. The median limiting magnitudes in each of the five bands corresponding to 5σ source detection limits are approximately 21.0, 23.1, 22.4, 21.4, 20.2. The details of the VST image processing and the catalogue assembly can be found in Koposov et al. (2014). For the analysis presented in this paper, we have transformed ATLAS Vega magnitudes to AAVSO Photometric All-Sky Survey (APASS) AB system by adding -0.031 , 0.123 and 0.412 to the *g*-, *r*- and *i*-band magnitudes, respectively. Subsequently all of these magnitudes are corrected for Galactic extinction using the dust maps of Schlegel, Finkbeiner & Davis (1998).

2.2 Discovery

Crater was discovered in 2013 October during a systematic search for stellar overdensities using the entirety of the ATLAS data processed to that date (~ 2700 deg²). The satellite stood out as the most significant candidate detection, as illustrated by the second panel of Fig. 1 showing the stellar density distribution around the centre of Crater. In this map, the central pixel corresponds to an overdensity in excess of 11σ over the Galactic foreground. The identification of the stellar clump as a genuine Milky Way

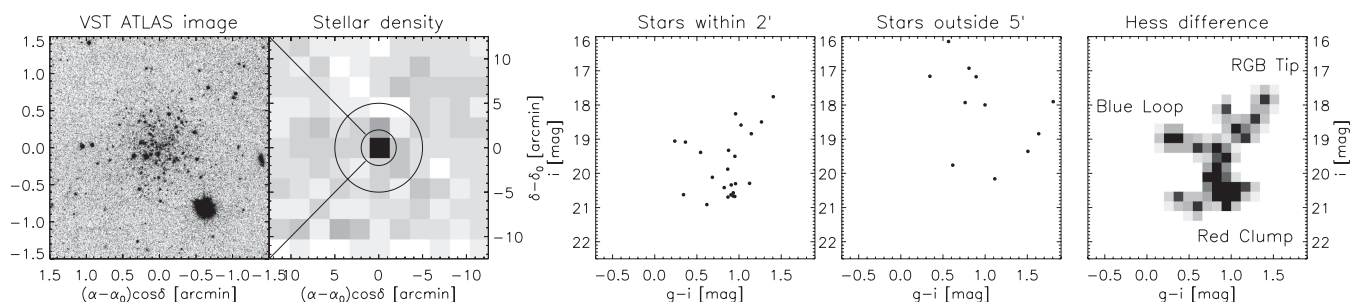


Figure 1. Discovery of the Crater satellite in VST ATLAS survey data. First: 3×3 arcmin² ATLAS *r*-band image cut-out of the area around the centre of the satellite. Second: stellar density map of a 25×25 arcmin² region centred on Crater and smoothed using a Gaussian kernel with FWHM of 2 arcmin. Darker pixels have enhanced density. The smaller circle marks the region used to create the CMD of the satellite stars. Bigger circle denotes the exclusion zone used when creating the CMD of the Galactic foreground. Third: CMD of the 2 arcmin radius region around the centre of Crater. Several coherent features including a RGB and RC are visible. Also note several stars bluer and brighter than the RC. These are likely BL candidate stars indicating recent (< 1 Gyr) star formation activity in the satellite. Fourth: CMD of the Galactic foreground created by selecting stars that lie outside the larger circle marked in the second panel and covering the same area as that within the small circle. It appears that the satellite CMD is largely unaffected by Galactic contamination. Fifth: Hess difference of the CMD density of stars inside the small circle shown and stars outside the large circle.



Figure 2. False-colour WHT ACAM image cut-out of an area 4×4 arcmin² centred on Crater. The i -band frame is used for the red channel, r -band for the green and g -band for the blue. The image reveals the dense central parts of Crater dominated by faint MSTO and SGB stars. Several bright stars are clearly visible, these are the giants on the RGB and in the RC. Amongst these are three or four bright BL giant candidates. A sprinkle of faint and very blue stars is also noticeable. These are likely to be either young MS stars or BSs.

satellite was straightforward enough as the object was actually visible on the ATLAS frames¹ as evidenced by the first panel of Fig. 1. The colour–magnitude diagram (CMD) of all ATLAS stars within 2 arcmin radius around the detected object is presented in the third panel of the figure. There are three main features readily discernible in the CMD as well as in the accompanying Hess difference diagram (shown in the fifth panel of the figure). They are the red giant branch (RGB) with $18 < i < 21$, the red clump (RC) at $i \approx 20.5$ and the likely blue loop (BL) giants, especially the two brightest stars with $g - i < 0.5$ and $i \approx 19$. While the identification of these stellar populations seems somewhat tenuous given the scarcity of the ATLAS CMD, it is supported by the deeper follow-up imaging, as described below.

2.3 Follow-up imaging with the WHT

The follow-up WHT imaging data were taken using the Cassegrain instrument Auxiliary-port Camera (ACAM) in imaging mode. The observations were executed as part of a service programme on the night of 2014 February 11 and delivered 3×600 s dithered exposures in the g , r and i bands with seeing of around 1 arcsec. The effective field-of-view of ACAM is some 8 arcmin in diameter with a pixel scale of 0.25 arcsec pixel^{−1}.

A series of bias and twilight flat frames taken on the same night were used to bias correct, trim and flat-field the data. Fringing, even on the i -band images, was negligible. Fig. 2 shows a false-colour image cut-out created using the ACAM i -, r - and g -band frames for

the red, green and blue channels, respectively. This 4×4 arcmin² fragment reveals the dense central parts of the satellite. Concentrated around the middle are a handful of bright stars (saturated in this false-colour image and therefore appearing white). As the following section makes clear, these are the RGB stars, RC giants and possible BL giants. The fainter white stars are the main-sequence turnoff (MSTO) dwarfs. Also visible in this image are faint and very blue stars which must be either a young MS or the blue straggler (BS) population.

Object catalogues were generated from the processed images to refine the world coordinate system transformation. Each set of three individual dithered exposures per band were then stacked with bad pixel and cosmic ray rejection and further catalogues from the combined images generated. These catalogues were then morphologically classified and the photometry cross-calibrated with respect to the VST ATLAS g -, r - and i -band data, yielding the CMD shown in Figs 3, 7 and 8. While overall, the innards of Crater appear resolved in the ACAM images, the resulting photometry does suffer from blending problems to some extent. Therefore, in the following analysis we use two versions of the WHT stellar catalogues. First, the most stringent sample (sample A) is created by requiring that each object is classified as stellar in both r and i frames. This produces clean photometry across the face of the satellite, but leads to a pronounced depletion in the very core. The total is 1271 star-like objects across the ACAM frame and 324 within $2r_h$. We use this catalogue for the CMD studies. Alternatively, if a more relaxed condition of being detected in one of the three of the g , r or i bands is applied, the total of 1964 (496 inside $2r_h$) objects classified as stars is recovered. We use this sample (sample B) to study the density distribution and to measure the structural parameters of Crater, including its luminosity. Note that the ratios of the objects in each of the two catalogues also reflect the relative decrease in the number of genuine background galaxies in the more stringent sample. If no morphological classification is enforced, there are 2228 objects in total across the ACAM frame, with 550 objects inside $2r_h$.

3 PROPERTIES OF CRATER

3.1 Distance

The best distance indicator available amongst the stellar populations in Galactic satellites is the blue horizontal stars (BHS), either stable or pulsating, i.e. RR Lyrae. Unfortunately, as Section 3.3 demonstrates, these are not present in Crater. However, the newly discovered satellite possesses a well-defined RC. Therefore, we endeavour to estimate Crater’s heliocentric distance by calibrating the average intrinsic luminosity of its RC stars with the extant photometry of similar stellar populations in the dwarf galaxies with known distances. To this end we take advantage of the publicly available treasure trove of broad-band photometry of the Local Group dwarf galaxies observed with the *Hubble Space Telescope* (HST) described in Holtzman et al. (2006). We chose five dwarfs with prominent RC and/or red horizontal branch (RHB) populations, namely Fornax, Draco, Carina, Leo II and LGS 3. To compare the WHT data to the HST photometry, we transform the APASS AB g and i magnitudes of Crater stars to V and I magnitudes using the standard equations of Lupton.²

To select the RGB and the RC/RHB stars in the above-mentioned galaxies, we apply the colour–magnitude mask shown in Fig. 3

¹ In fact, Crater is visible on the Digitized Sky Survey images as well, similarly to Leo T.

² <http://www.sdss.org/dr7/algorithms/sdssUBVRITransform.html>

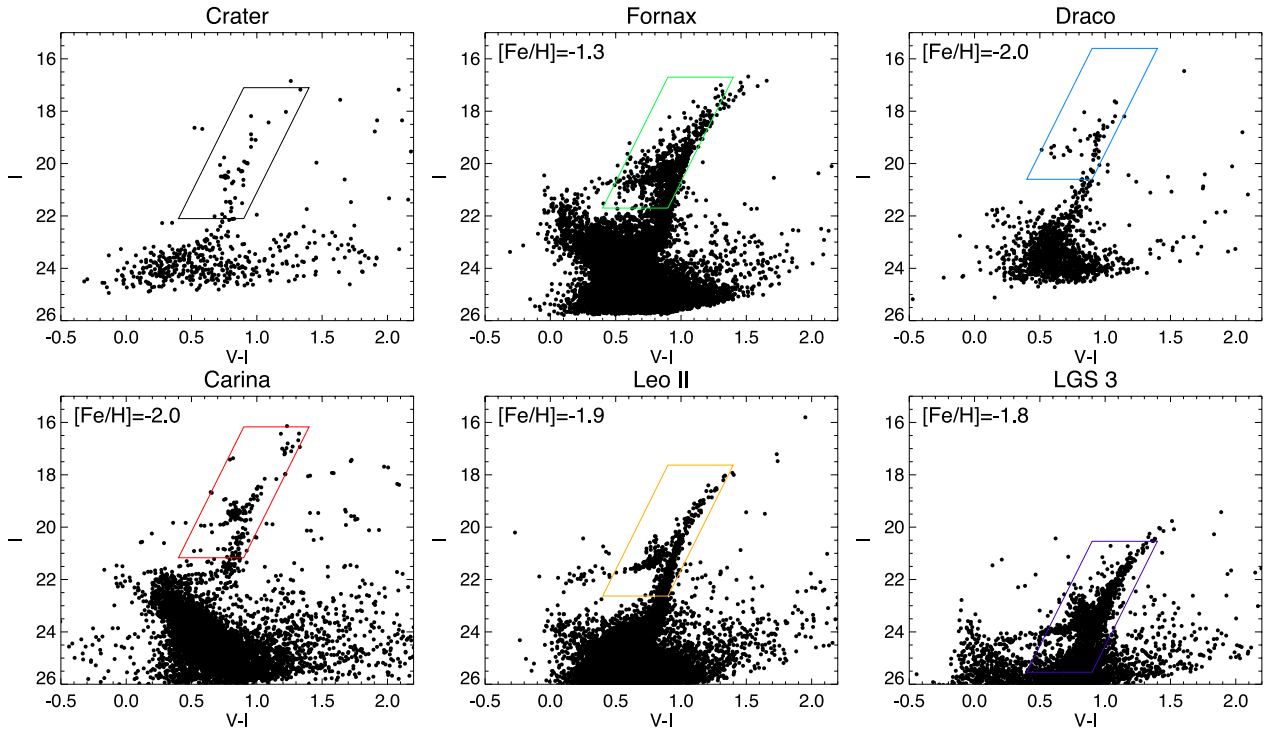


Figure 3. RC morphology. The CMD features around the RC region in Crater (top left) are contrasted to those in five classical dwarf galaxies observed with the *HST* (Holtzman, Afonso & Dolphin 2006). The polygon mask shows the boundary used to select the RC/RHB and RGB stars for the luminosity function comparison in Fig. 4. The RC/RHB region of Crater most closely resembles that of Carina, the main differences being the lack of an obvious HB and the presence of a small but visible BL extension. Top centre: Fornax, at $(m - M) = 20.7$ and $E(B - V) = 0.025$. Top right: Draco, at $(m - M) = 19.6$ and $E(B - V) = 0.03$. Bottom left: Carina, at $(m - M) = 20.17$ and $E(B - V) = 0.06$. Bottom centre: Leo II, at $(m - M) = 21.63$ and $E(B - V) = 0.017$. Bottom right: LGS 3, at $(m - M) = 24.54$ and $E(B - V) = 0.04$. The dwarf photometry is extinction corrected.

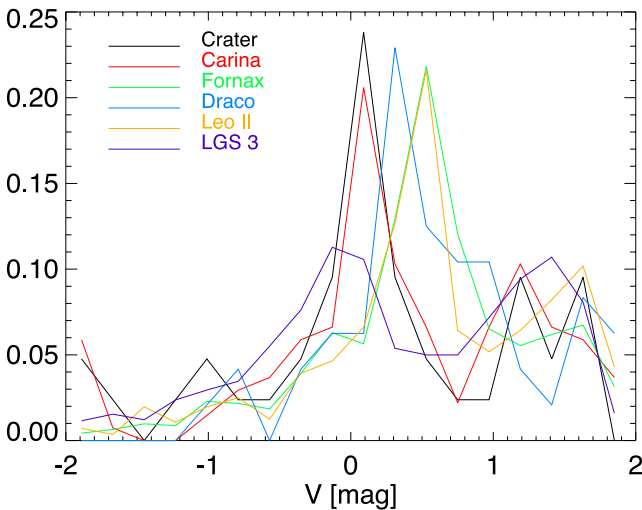


Figure 4. LFs of stars selected using the polygon CMD masks in six satellites as shown in Fig. 3, given the distance moduli and the extinction values recorded in Fig. 3 caption. The difference in RC/RHB morphology is reflected in the difference of LF shapes and, most importantly, in different absolute magnitudes of the LF peak. Crater's stars are offset to $(m - M) = 21.1$ to match the peak of Carina's LF.

offset to the appropriate distance modulus (listed for each object in the figure caption). The colour of the polygon used for selection corresponds to the colour of the luminosity function (LF) curve shown for each dwarf galaxy in Fig. 4. As evident from Fig. 3, the morphology of the RC/RHB is subtly (but noticeably) different in each

case. This is reflected in the shape of the LF in Fig. 4. For example, Draco, Fornax and Leo II have a property in common: a substantial RHB, pushing the peak of the RC/RHB region faintwards. This is to be compared with LGS 3 which exhibits a noticeable stump of BL stars extending from RC/RHB to brighter magnitudes at bluer $V - I$. As a result, in LGS 3 the RC/RHB LF peaks some 0.7 mag brighter as compared to Leo II and Fornax. Morphologically, the RC/RHB of Carina appears to be the closest match to Crater's. Carina's RC/RHB LF reaches a maximum at $M_V = 0.1$, which gives $(m - M) = 21.1$, or ~ 170 kpc for the distance of Crater.

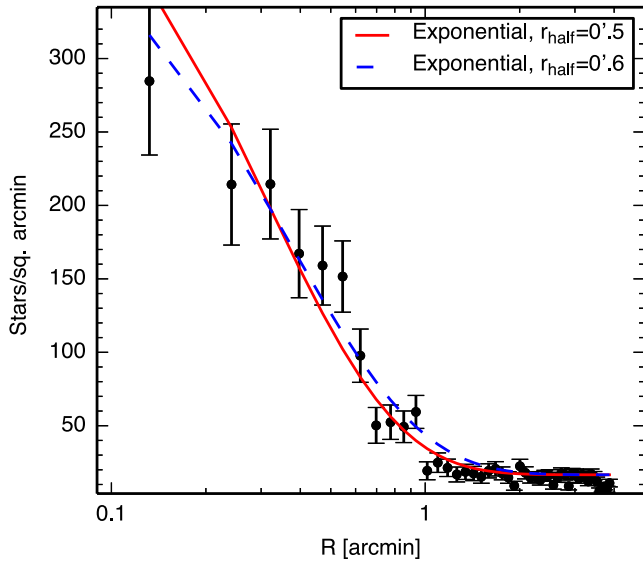
Alternatively, it is possible to gauge the distance to the new satellite by taking advantage of the gently sloping correlation between the absolute magnitude of the horizontal branch (HB) and the metallicity established for the Galactic GCs. As apparent from comparison of the panels in Fig. 3, the Crater RGB is bluer and steeper compared to most of the dwarf spheroidal populations displayed. Therefore, as an initial estimate, the plausible metallicity range could be as low as $[\text{Fe}/\text{H}] < -1.8$. According to the study of Dotter et al. (2010), for a GC of low metallicity $M_V^{\text{HB}} \sim 0.4$ which would bring Crater slightly closer to the Sun at $(m - M) = 20.8$, or 145 kpc. As Section 3.3 details, Crater's CMD does indeed appear consistent with an old metal-poor stellar population. Note, however, that no GC with $[\text{Fe}/\text{H}] < -1$ in the sample analysed by Dotter et al. (2010) boasts as red a HB as that found in Crater.

3.2 Size and luminosity

The structural properties of Crater are measured through maximum likelihood (ML) modelling (see e.g. Martin, de Jong & Rix 2008)

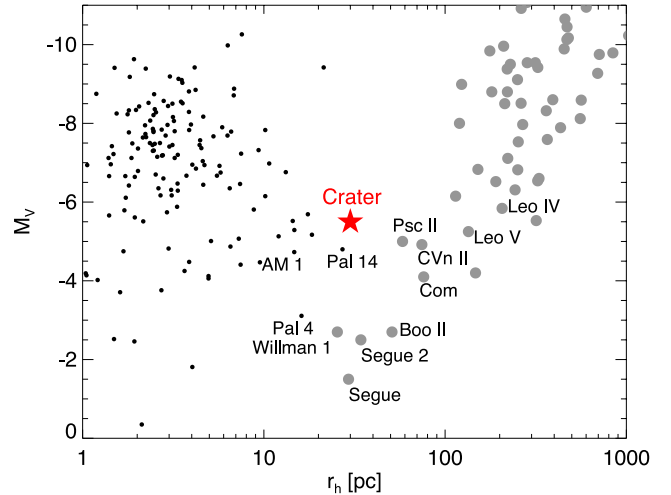
Table 1. Properties of the Crater satellite.

Property	
Coordinates (J2000)	$\alpha = 11:36:15.8, \delta = -10:52:40$
Coordinates (J2000)	$\alpha = 174^\circ 066, \delta = -10^\circ 8777$
Coordinates (Galactic)	$\ell = 274^\circ 8, b = 47^\circ 8$
Ellipticity	0.08 ± 0.08
r_h (exponential)	0.6 ± 0.05 arcmin
V_{tot}	15.8 ± 0.2 mag
$(m - M)_0$	$20.8 - 21.1$ mag
$M_{\text{tot},V}$	-5.5 ± 0.5 mag

**Figure 5.** Surface brightness profile of stars in the ACAM sample B with $i < 24.5$ (black). Overlaid are exponential density models with half-light radius of $r_h = 0.5$ arcmin (red, solid) and $r_h = 0.6$ arcmin (dashed, blue).

of the positions of stars with $g - i < 1.6$ selected from the ACAM sample B. The results of the ML analysis are reported in Table 1. While the nominal error on the half-light radius is rather small, given that the central parts of Crater suffer from some amount of blending, it could perhaps be slightly overestimated. Note however that switching from sample B to A, i.e. losing as much as ~ 35 per cent of star-like objects within $2r_h$ leads only to a minor increase in half-light radius from 0.6 to 0.7 arcmin. We have investigated further the effects completeness might have on the stellar density profile parametrization. If the sample B is limited to stars brighter than $i = 24.5$, i.e. objects less affected by blending, then the structural parameters of Crater evolve as follows. For the brighter sample, we get r_h between 0.5 and 0.55 arcmin and the ellipticity of 0.2 ± 0.05 at the position angle of 110° . As Fig. 5 illustrates, the exponential profile with half-light radius between $r_h = 0.5$ and 0.6 arcmin is a reasonable fit to the ACAM data. Note that at a distance of 170 kpc, 0.6 arcmin corresponds to 30 pc (or 25 pc at 145 kpc). Depending on the tracer sample used, the density flattening is either consistent with zero (all stars) or very slight elliptical (bright cut). For further analysis, we chose to assume the ellipticity of Crater to be zero. The question of the satellite's true shape can only be resolved with a higher resolution data set.

To estimate the total luminosity of the satellite, we sum up the flux of all sample B stars inside $3r_h$ that fall within a generous colour-magnitude mask enclosing the MSTO, the RGB, the RC and the BL. The total is $V_{\text{tot}} = 15.8$, for a miniscule foreground con-

**Figure 6.** Luminosity M_V versus half-light radius r_h for Galactic GCs (black dots) and Milky Way and M31 satellites (grey circles). The red star marks the location of Crater. The new satellite appears to have more in common with the Galactic GC population, even though it appears to be the largest of all known Milky Way globulars. Contrasted with the known ultrafaint satellites, Crater is either too small for the given luminosity, cf. Pisces II, Leo V or too luminous for a given size, cf. Willman 1, Segue.

tamination of 18 mag. Therefore, assuming the distance modulus of $(m - M) = 21.1$, the total luminosity of Crater down to the MSTO is $M_V = -5.2$. By integrating the LF of the old and metal-poor GC M92 faintwards of the turn-off, we obtain the correction of ~ 0.3 mag in missing flux, giving the final estimate of the total luminosity $M_V = -5.5$. This is likely to be the lower bound as we have not accounted for the stars missing from sample B due to blending or any additional populations fainter than the detected MSTO.

As Fig. 6 illustrates, at $M_V = -5.5$ and $r_h = 30$ pc, Crater looks more like a puffed up GC rather than a dwarf spheroidal galaxy. In the Milky Way there are examples of faint and extended clusters that might superficially resemble Crater, for example, Palomar 14, which is only ~ 1 mag less luminous. The only known galaxies that have some properties in common with Crater are the so-called ultrafaint dwarfs (UFDs). These, however are either much bigger at the same luminosity like Pisces II or Leo V, or much fainter at the same size like Willman 1 or Segue. Of course, the total luminosity and the extent of the stellar distribution alone do not determine the satellite's nature. While many previously existing boundaries have been blurred with the discovery of the UFDs, an extended star formation history generally counts as a feature inherent to galaxies and not star clusters. That being the case, it is worth taking a closer look at the stellar populations of Crater.

3.3 Stellar populations

Fig. 7 gives the positions on the CMD of all stars in sample A located within two half-light radii from the Crater's centre. The ACAM photometry reaches as faint as $i \sim 25$, the depth sufficient to detect the sub-giant branch (SGB) and the MSTO at ~ 170 kpc. As the Hess difference (shown in the right-hand panel of the figure) emphasizes, the SGB is very tight. To put constraints on the metallicity and the age of the system, three sets of Dartmouth isochrones (Dotter et al. 2008) with different metallicities are also overplotted. For each of the three values of $[\text{Fe}/\text{H}]$ (-2.5 , -2 and -1.5 corresponding to blue, green and red curves), two ages are shown, namely 7 and 10 Gyr. If the RC distance calibration is correct, then the bulk of

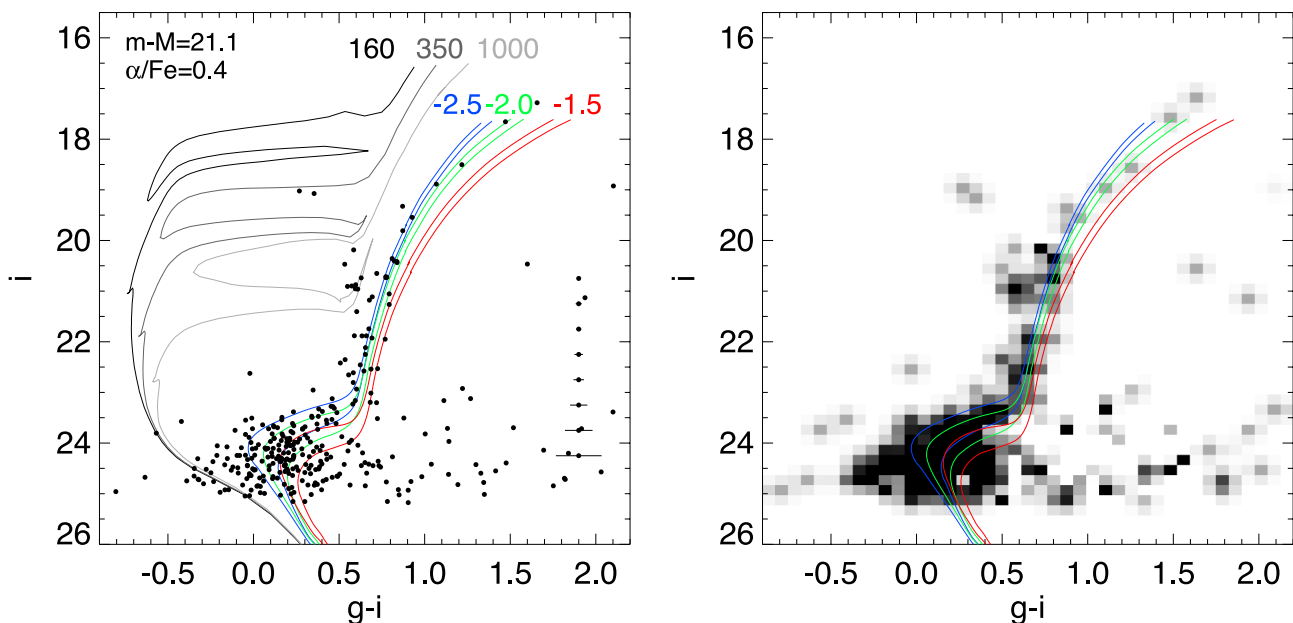


Figure 7. CMD of the Crater stars within $2r_h$ of the centre. Left: all WHT ACAM sample A stars inside two half-light radii. For comparison, 7 and 10 Gyr and $[\alpha/\text{Fe}] = 0.4$ Dartmouth isochrones with metallicities $[\text{Fe}/\text{H}] = -2.5$ (blue), $[\text{Fe}/\text{H}] = -2.0$ (green) and $[\text{Fe}/\text{H}] = -1.5$ (red) are overplotted. Also shown are 160 Myr (black), 350 Myr (dark grey) and 1 Gyr (light grey) Padova isochrones. If the RC distance calibration is trustworthy, then the bulk of Crater’s stellar population is old (between 7 and 10 Gyr) and metal poor ($-2.5 < [\text{Fe}/\text{H}] < -2.0$). However, there are three peculiar stars, two directly above the blue side of the RC and one at $g-i \sim 0.3$ and $i \sim 19$ that can be interpreted as BL giants. If this interpretation is correct, then according to the Padova isochrones, Crater has experienced a small amount of star formation around 1 Gyr ago and perhaps as recently as 350 Myr ago. Right: Hess difference between the CMD densities of the stars inside r_h and the stars outside $4.5r_h$. Note the tightness of the subgiant region.

Crater’s stellar content has to be metal poor, i.e. somewhere between $[\text{Fe}/\text{H}] = -2.5$ and -2.0 and old, i.e. with an age between 7 and 10 Gyr.

Fig. 7 also reveals four stars, bluer and brighter than the RC. Two of these are directly above the RC location at $i \sim 20.5$, and the two bluest ones are at $i \sim 19$. We interpret these bright and blue stars as belonging to the core helium burning BL population. As the name suggests, the colour and the luminosity of the BL stars vary markedly during their lifetime. However, their peak luminosities are robust indicators of age and as such BL stars have been used successfully to map star formation histories in dwarf galaxies (e.g. Tolstoy et al. 1998). According to the Padova isochrones (Girardi et al. 2004) overplotted in the left-hand panel of Fig. 7, the age of the two faint BL stars is of order of 1 Gyr while the brightest one is somewhat younger at ~ 400 Myr. Fig. 9 shows the distribution of the BL candidates in and around Crater. According to the figure, there is very little Galactic contamination from stars with colours and magnitudes typical of the Crater’s BL and RC populations.

If it were not for the presence of the handful of possible BL giants, classifying the new satellite would be easy as it has more features in common with the currently known Galactic GCs than with classical or UFDs. Spectroscopic follow-up is needed to firmly establish whether the BL candidates are indeed members of Crater and not mere Galactic foreground contaminants. Surprisingly, Fig. 7 does not include the low-mass MS counterparts to the more massive BL stars discussed above. Fig. 8 helps to explain why. To be included into sample A, objects must be classified as stellar in both r and i bands.³ However, for a young MS star, most of the flux would be

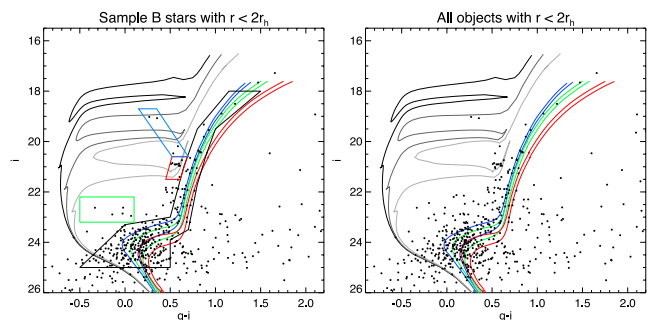


Figure 8. CMD evolution with morphological classification. Left: CMD of objects inside $2r_h$ in sample B. Compared to the sample of stars with cleanest photometry (sample A) shown in Fig. 7, the CMD looks almost identical at magnitudes brighter than that of the RC. However, faintwards of the RC there are noticeable differences. Note several faint blue stars above the MSTO. These are either young MS stars or BSs. Also shown are CMD masks used to select the MSTO/RGB (black), RC (red), BL (blue) and young MS (green) populations. The distribution of the selected stars on the sky is shown in Fig. 9. Right: CMD of all objects within $2r_h$. The region directly above the MSTO is now densely populated. Most likely, the photometry of these stars have been affected by blending, more precisely, given their colours and magnitudes by blending of YMS/BS stars and SGB/RGB populations.

detected in the g band. The left-hand panel of the figure shows the CMD of all sample B objects (i.e. objects classified as stars in r , i or g bands) within $2r_h$. A group of several blue stars is clearly visible above the MSTO (also see Fig. 9). The right-hand panel of the figure shows the CMD for all objects inside $2r_h$ independent of their morphological classification. The region above the MSTO is now more densely populated. Given the colours and the magnitudes of these objects, they could be young MS (or BS) stars blended with SGB/RGB population. Therefore, it seems that there could

³ Unfortunately the seeing in the g -band data was substantially worse compared to r and i .

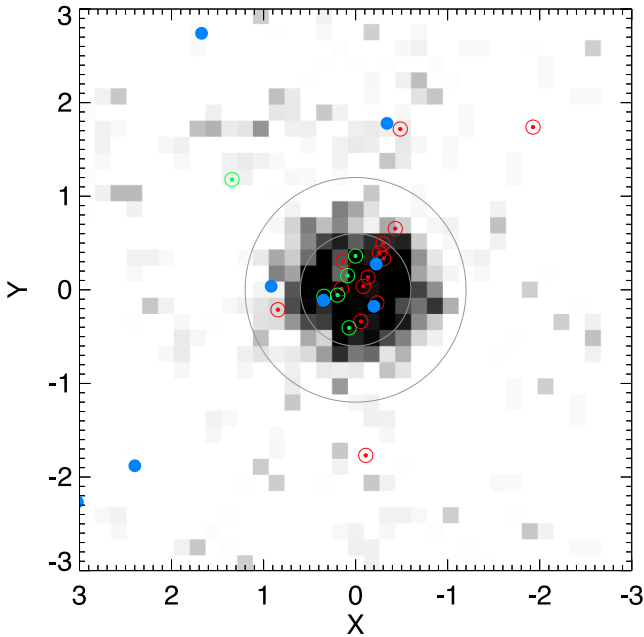


Figure 9. Distribution of Crater stars on the sky for three populations selected using the CMD masks shown in the bottom right-hand panel of Fig. 8. The grey-scale reflects the density distribution of the MSTO stars. Red circles mark the locations of the RC giants, blue filled circles are BL stars and green circles are young MS candidates. Large grey circles give the r_h and $2r_h$ boundaries.

be a substantial young MS population in Crater corresponding to the handful of more massive BL giants. Considering the blending problems affecting photometry in the central parts, higher resolution imaging is required to further probe the CMD of the satellite.

3.4 Peculiar globular cluster?

Without spectroscopic follow-up, it is not possible to judge adequately the probability of the satellite membership for the handful of bright blue stars in and around Crater. Leaving aside the issue of the possible BL, how does Crater fare in comparison to the known Galactic globulars? A different attempt to find a match for the satellite's stellar populations is shown in Fig. 10. Here, a set of Dartmouth isochrones similar to those in Figs 7 and 8 is

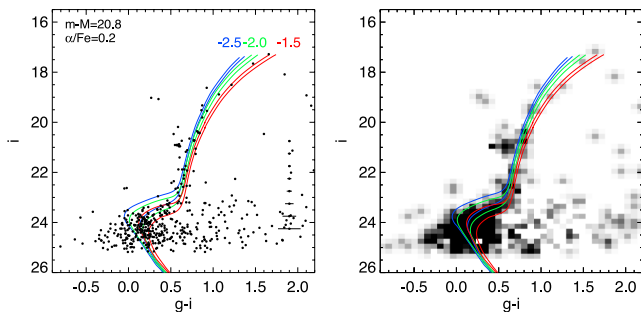


Figure 10. See Fig. 7 for detail. Left: CMD of star-like objects inside $3r_h$ in sample A. Compared to Fig. 7, a lower (more cluster-like) distance modulus is assumed ($m - M$) = 20.8 as well as a lower enhancement for the Dartmouth isochrones $[\alpha/\text{Fe}] = 0.2$. The change in distance and in the light elements budget results in a slightly better agreement with the metal-rich isochrones. However, the RGB of a population with $[\text{Fe}/\text{H}] = -1.5$ remains too red compared to Crater's.

overplotted. However, this time a lower (more cluster-like) distance modulus is assumed ($m - M$) = 20.8 as well as lower $[\alpha/\text{Fe}] = 0.2$ enhancement. With these adjusted parameters, the distinction between $[\text{Fe}/\text{H}] = -2.0$ and -1.5 is less obvious. However, the isochrone with $[\text{Fe}/\text{H}] = -1.5$ still lies to the red of the Crater's RGB.

The disagreement between the model $[\text{Fe}/\text{H}] = -1.5$ population and the Crater photometry is even more striking given how red its HB is. The richness of the morphology of the HB in GCs has yet to be explained, but it is well established that stubby and red HBs resembling RCs are a prerogative of metal-rich globulars. Note that the RC itself is rarely invoked in the analysis of a GC as it assumes the existence of multiple stellar populations with different ages. Metallicity is the primary driver of the HB morphology with several other contenders for the less important second and even third parameters. For example, Dotter et al. (2010) measure the difference in the median $V - I$ colour of the HB and the corresponding piece of the RGB for a large sample of Galactic GCs with available *HST* photometry and show that age could perhaps play the role of the second parameter, while the central cluster density acts as a third. The study of Dotter et al. (2010) shows off beautifully the previously identified dichotomy between the inner and outer cluster populations in the Milky Way. It appears that while following the trend overall, at given metallicity the two subsamples show distinct colours and extents in their HBs: short red HBs (with low $\Delta(V - I)$ values) typically correspond to metal-rich globulars in the inner Galaxy, but also can be found in relatively metal-poor systems in the outer halo.

The most conspicuous examples of this dichotomy are found in the few most distant (i.e. beyond 80 kpc) and extended GCs, such as Pal 4, Pal 14 and AM-1. As obvious from fig. 10 of Dotter et al. (2010), the HB-*RGB* colour difference $\Delta(V - I)$ in these reaches values as low as 0.2. Interestingly, at the same $\Delta(V - I)$, the inner clusters are found to be significantly more metal rich by at least 0.6 dex. Fig. 11 compares the CMD of Crater to the stellar populations in Pal 4 and Pal 14. Of the entire population of the Galactic GCs, these two are perhaps the closest matches to Crater's CMD morphology. Both are relatively metal poor and both have short red HBs. However, as Fig. 11 convincingly demonstrates neither matches Crater's CMD perfectly. First, the Crater RGB is clearly bluer than the RGB in either Pal 4 or Pal 14 which means that Crater ought to be more metal poor compared to these two. Judging by the offset between the Crater RGB and the ridgelines of Pal 4 and Pal 14, our original estimate that the its metallicity is lower than -1.5 , and perhaps closer to -2.0 , must not be far from the truth. Secondly, the difference between the median colours of the HB and the RGB in Crater is even smaller than in Pal 4 and Pal 14, at $\Delta(V - I) = 0.11$. Fig. 12 is the analog of fig. 10 in Dotter et al. (2010) and aims to illustrate the unusual properties of the HB in Crater, assuming the satellite is a GC. According to this only a handful of the most metal-rich GCs in the Galaxy have a RHB situated that close to the RGB.

3.5 Companions

Curiously, Crater lies only $\sim 10^\circ$ away from two recently discovered ultrafaint satellite of the Galaxy: Leo IV which itself is accompanied by Leo V some 2° further to the north (see Fig. 13). The distances to all three satellites agree within the likely errors, therefore, there seems to be an interesting bunching of satellites over a relatively small area of sky at $160 < D < 180$ kpc distance. As Fig. 13 illustrates, it is possible to draw a great circle, namely with the pole

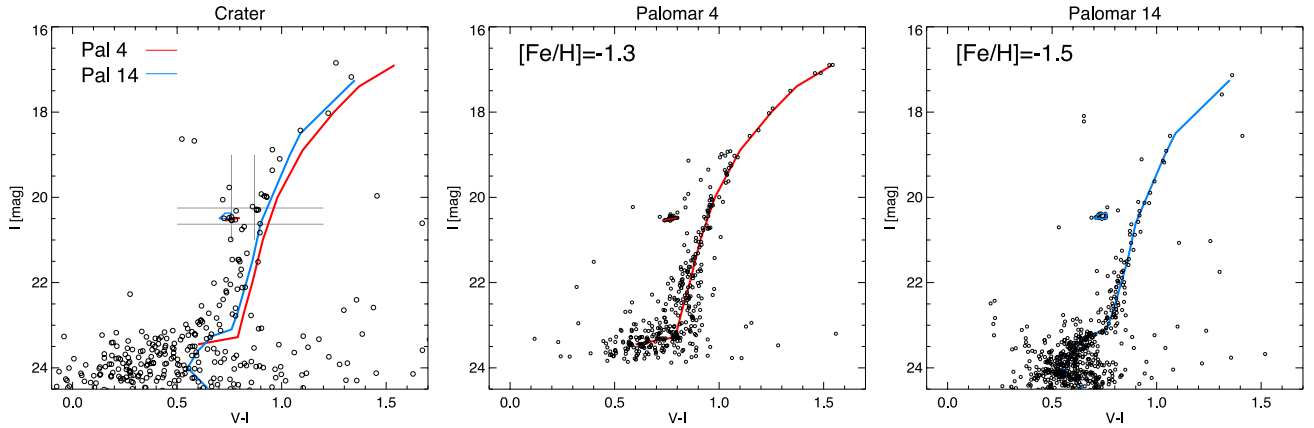


Figure 11. Crater’s CMD compared to two extreme outer halo GCs Pal 4 (at $(m - M) = 20.21$) and Pal 14 (at $(m - M) = 19.54$). The Pal 4 and Pal 14 distances are from Dotter et al. (2010). Left: CMD of star-like objects inside $2r_h$ in sample A. Blue (red) line shows the ridgeline of Pal 14 (Pal 4) offset to $(m - M) = 20.8$. We conclude that Crater must be more metal poor than $[\text{Fe}/\text{H}] = -1.5$ as both ridgeline RGBs are clearly redder. Note that the apparent magnitudes of the RHBs of both Pal 4 and Pal 14 match very well the location of the RC/RHB in Crater, lending support to our distance determination. Grey horizontal lines show the stars selected for the $\Delta(V - I)$ measurement. Grey vertical lines show the median $V - I$ colours of the RC/RHB and RGB stars selected, resulting in the value of $\Delta(V - I) = 0.11$. Middle: CMD of Pal 4 stars from Saha et al. (2005) offset to the distance $(m - M) = 20.8$. The red line shows the approximate ridgeline. Right: CMD of Pal 14 stars from Saha et al. (2005) offset to the distance $(m - M) = 20.8$. The blue line shows the approximate ridgeline.

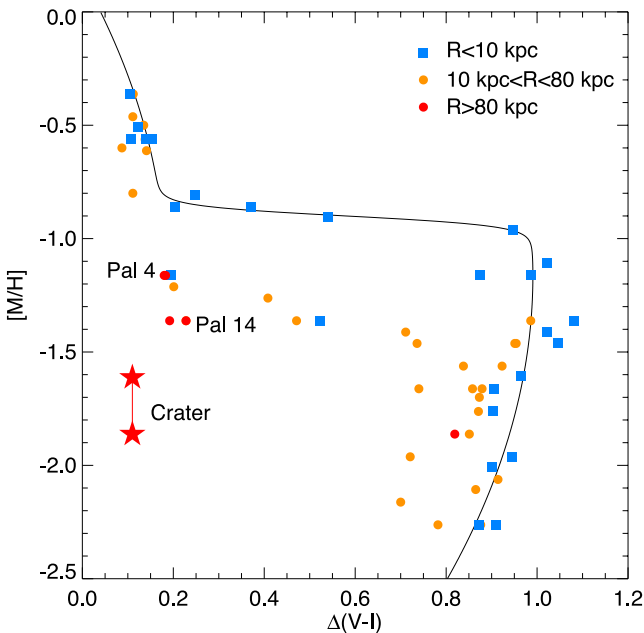


Figure 12. Morphology of the HB as a function of metallicity in Galactic GCs. This shows metallicity $[\text{M}/\text{H}] = [\text{Fe}/\text{H}] + \log_{10}(0.638 \times 10^{[\alpha/\text{Fe}]} + 0.362)$ as a function of the difference in median colour between the HB and the RGB $\Delta(V - I)$. Blue squares mark the locations of the inner globulars, while orange circles indicate the outer GCs. Red circles show the properties of the most distant GCs including Pal 4 and Pal 14. The solid black line is a fit from Dotter et al. (2010). Note that the HB morphology in Crater is rather unusual compared to the rest of the Milky Way population: it is too red and too short (i.e. much more RC-like) for its metallicity.

at $(\alpha, \delta) = (83^\circ.1, -5^\circ.3)$, that will pass very near Crater, Leo IV and Leo V.

de Jong et al. (2010) have already found evidence for a stellar bridge connecting Leo IV and Leo V. They show that if the Milky Way’s potential is spherical, then Leo IV and Leo V do not share the exact same orbit, but conclude that the galaxies are most

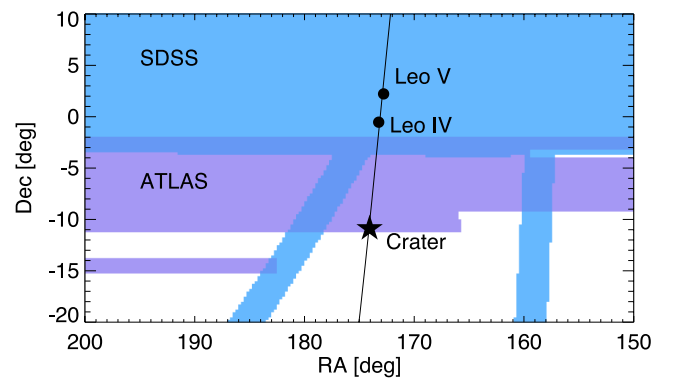


Figure 13. Large-scale view of Crater’s position on the sky. Curiously, Crater, at 170 kpc, appears to lie only $\sim 10^\circ$ away from the Leo IV (155 kpc) satellite which itself is a neighbour of Leo V (180 kpc). The blue region gives the footprint of the SDSS survey in which Leo IV and Leo V were discovered, while purple shows the boundaries of the current ATLAS VST footprint in this region. The black line is the great circle passing very close to all three satellites and with a pole at $(\alpha, \delta) = (83^\circ.1, -5^\circ.3)$.

likely an interacting pair that fell into the Milky Way halo together. Although the infall of groups or associations of dwarfs seems the most probable explanation, it merits further investigation whether such an alignment could still be purely accidental.

To complement Fig. 13, Fig. 14 gives the positions of all classical and ultrafaint satellites on the sky in Galactic coordinates. It is perhaps worth noting that the ultrafaint satellites UMa I and Willman I also lie close to the great circle passing through Crater, Leo IV and Leo V.

4 CONCLUSIONS

In this paper we have presented the discovery of a new Galactic satellite found in VST ATLAS survey data. The satellite is located in the constellation of Crater (the Cup) and has the following properties.

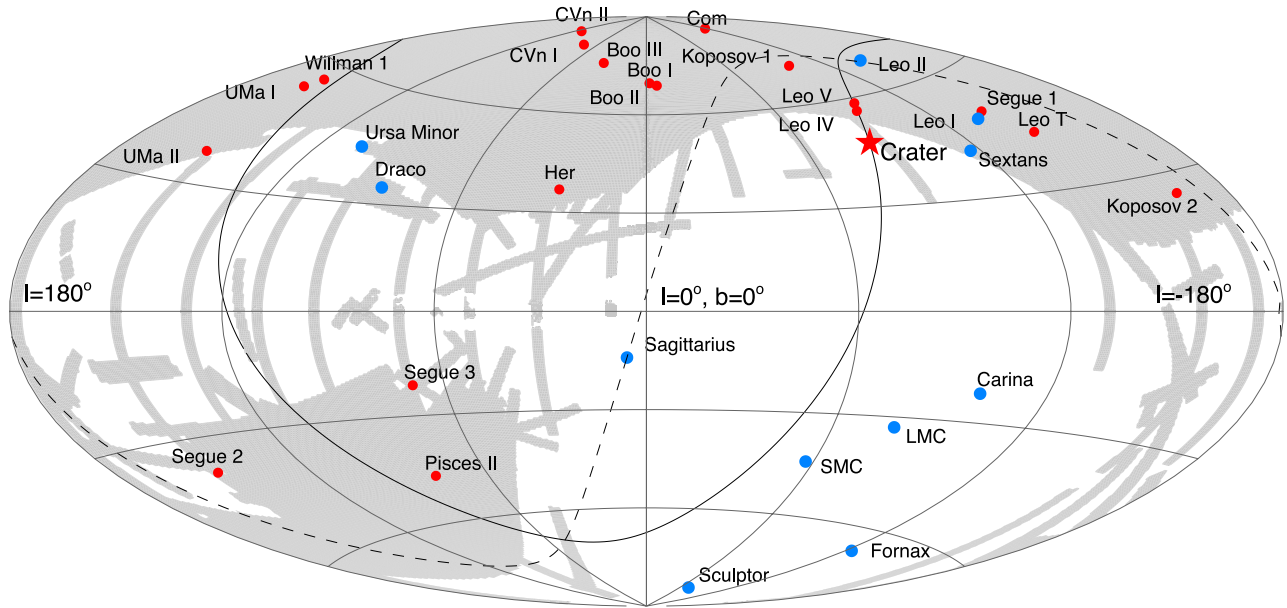


Figure 14. Positions of the classical (blue circles) and ultrafaint (red circles) satellites on the sky. The dashed curve shows the orbit of the Sgr dwarf, while the solid line represents the great circle with pole at $(\alpha, \delta) = (83^\circ 1, -5^\circ 3)$ passing through Crater, Leo IV and Leo V.

(1) The satellite has a half-light radius of $r_h \sim 30$ pc and a luminosity of $M_V = -5.5$.

(2) The heliocentric distance to Crater is between 145 and 170 kpc.

(3) The bulk of Crater's stellar population is old and metal poor.

(4) However, there are also several bright blue stars that appear to be possible Crater members. We interpret these as core helium burning BL giants and, therefore, conclude that the satellite might have formed stars as recently as 400 Myr ago.

(5) If Crater were a GC then it possesses the shortest and the reddest HB of all known Galactic globulars with $[\text{Fe}/\text{H}] < -1$. Such a stubby RHB could otherwise be confused with a RC.

If our hypothesis of relatively recent star formation is correct, then Crater must be classified as a dwarf galaxy, as no extended star formation has ever been recorded in GCs. The satellite then clearly stands out compared to the rest of the known dwarfs, both classical and ultrafaint: it is much smaller and less luminous than the classical specimens and much denser than the typical ultrafaint ones. Given its feeble size and luminosity it is surprising to have found (albeit tentative) evidence for a younger population. The only other Galactic dwarf of comparable metallicity, age and luminosity, with detected low levels of recent star formation, is Leo T (Irwin et al. 2007; Ryan-Weber et al. 2008), which is known to have kept some of its neutral hydrogen supply intact. This is perhaps unsurprising given its large Galactocentric distance and very modest levels of star formation activity. We have attempted a search for the presence of H I coincident with the location of Crater in the data of the Galactic All Sky Survey (GASS) radio survey (McClure-Griffiths et al. 2009), but found no convincing evidence for a stand-alone neutral hydrogen cloud. Based on the fact that the H I gas in Leo T is barely detected in the HI Parkes All Sky Survey (HIPASS) data (Irwin et al. 2007), and given that Crater is significantly less luminous compared to Leo T, it is perhaps worth pointing a radio interferometer in the direction of this satellite.

Crater is just the most recent in a series of discoveries of ambiguous objects that share some of the properties of clusters and dwarf galaxies. The discoveries of Willman 1 and Segue 1 were followed

by similar controversies as to their true nature (see e.g. Willman et al. 2005b, 2011; Niederste-Ostholt et al. 2009; Martinez et al. 2011). Philosophers of course recognize this as the fallacy of the excluded middle, in which a binary choice is assumed to exhaust all the possibilities. The question 'Is Crater a globular cluster or a dwarf galaxy?' might just be as futile as the question 'Is the platypus an otter or a duck?'. The egg-laying mammal looks like both but is neither. Instead, its mixed-up appearance is the result of it having evolved in an unusual and isolated location.

ACKNOWLEDGEMENTS

The authors wish to thank Emma Ryan-Weber for the expert advice regarding the GASS data. VB has enjoyed discussing the details of this work with Mario Mateo, Edward Olszewski, Daniel Weisz and Thomas de Boer. The research leading to these results has received funding from the European Research Council under the European Union's Seventh Framework Programme (FP/2007-2013)/ERC Grant Agreement no. 308024. Additionally, this research was made possible through the use of the AAVSO Photometric All-Sky Survey (APASS), funded by the Robert Martin Ayers Sciences Fund. VB acknowledges financial support from the Royal Society. SEK acknowledges financial support from the STFC and the ERC. VB and MJJ are indebted to the International Space Science Institute (ISSI), Bern, Switzerland, for supporting and funding the international team 'First stars in dwarf galaxies'.

REFERENCES

- Amorisco N., Evans N. W., 2012, *ApJ*, 756, 2
- Amorisco N., Evans N. W., van der Ven G., 2014, *Nature*, 507, 335
- Balbinot E. et al., 2013, *ApJ*, 767, 101
- Belokurov V., 2013, *New Astron. Rev.*, 57, 100
- Belokurov V. et al., 2006, *ApJ*, 647, L111
- Belokurov V. et al., 2007, *ApJ*, 654, 897
- Belokurov V. et al., 2008, *ApJ*, 686, L83
- Belokurov V. et al., 2009, *MNRAS*, 397, 1748
- Belokurov V. et al., 2010, *ApJ*, 712, L103

- Coleman M., Da Costa G. S., Bland-Hawthorn J., Martínez-Delgado D., Freeman K. C., Malin D., 2004, *AJ*, 127, 832
- Deason A. J. et al., 2011, *MNRAS*, 415, 2607
- de Jong J. T. A., Martin N. F., Rix H.-W., Smith K. W., Jin S., Macciò A. V., 2010, *ApJ*, 710, 1664
- D’Onghia E., Lake G., 2008, *ApJ*, 686, L61
- Dotter A., Chaboyer B., Jevremović D., Kostov V., Baron E., Ferguson J. W., 2008, *ApJS*, 178, 89
- Dotter A. et al., 2010, *ApJ*, 708, 698
- Fattahi A., Navarro J. F., Starkenburg E., Barber C. R., McConnachie A. W., 2013, *MNRAS*, 431, L73
- Girardi L., Grebel E. K., Odenkirchen M., Chiosi C., 2004, *A&A*, 422, 205
- Grillmair C. J., 2009, *ApJ*, 693, 1118
- Holtzman J. A., Afonso C., Dolphin A., 2006, *ApJS*, 166, 534
- Irwin M. J. et al., 2007, *ApJ*, 656, L13
- Koposov S. et al., 2007, *ApJ*, 669, 337
- Koposov S. et al., 2008, *ApJ*, 686, 279
- Koposov S. E., Yoo J., Rix H.-W., Weinberg D. H., Macciò A. V., Escudé J. M., 2009, *ApJ*, 696, 2179
- Koposov S. E., Irwin M., Belokurov V. et al., 2014, in press
- Kroupa P., Pawlowski M., Milgrom M., 2012, *Int. J. Modern Phys. D*, 21, 30003
- Li Y.-S., Helmi A., 2008, *MNRAS*, 385, 1365
- McClure-Griffiths N. M. et al., 2009, *ApJS*, 181, 398
- Martin N. F., de Jong J. T. A., Rix H.-W., 2008, *ApJ*, 684, 1075
- Martinez G. D., Minor Q. E., Bullock J., Kaplinghat M., Simon J. D., Geha M., 2011, *ApJ*, 738, 55
- Niederste-Ostholt M., Belokurov V., Evans N. W., Gilmore G., Wyse R. F. G., Norris J. E., 2009, *MNRAS*, 398, 1771
- Ryan-Weber E. V., Begum A., Oosterloo T., Pal S., Irwin M. J., Belokurov V., Evans N. W., Zucker D. B., 2008, *MNRAS*, 384, 535
- Saha A., Dolphin A. E., Thim F., Whitmore B., 2005, *PASP*, 117, 37
- Schlegel D. J., Finkbeiner D. P., Davis M., 1998, *ApJ*, 500, 525
- Tollerud E. J., Bullock J. S., Strigari L. E., Willman B., 2008, *ApJ*, 688, 277
- Tolstoy E. et al., 1998, *AJ*, 116, 1244
- Walsh S. M., Jerjen H., Willman B., 2007, *ApJ*, 662, L83
- Watkins L. L., Evans N. W., van de Ven G., 2013, *MNRAS*, 430, 971
- Willman B., Strader J., 2012, *AJ*, 144, 76
- Willman B. et al., 2005a, *ApJ*, 626, L85
- Willman B. et al., 2005b, *AJ*, 129, 2692
- Willman B., Geha M., Strader J., Strigari L. E., Simon J. D., Kirby E., Ho N., Warren A., 2011, *AJ*, 142, 128
- Zucker D. B. et al., 2006a, *ApJ*, 643, L103
- Zucker D. B. et al., 2006b, *ApJ*, 650, L41

This paper has been typeset from a \LaTeX file prepared by the author.